ADVANCES IN ATMOSPHERIC SCIENCES, VOL. 29, NO. 2, 2012, 391–406

An Investigation of the Effects of Wave State and Sea Spray on an Idealized Typhoon Using an Air–Sea Coupled Modeling System

LIU Bin[1,2] (刘 斌), GUAN Changlong*[2] (管长龙), Li'an XIE[1], and ZHAO Dongliang[2] (赵栋梁)

[1]*Department of Marine, Earth and Atmospheric Sciences, North Carolina State University, Raleigh, NC* 27695*, USA*

[2]*Physical Oceanography Laboratory, Ocean University of China, Qingdao* 266100

(Received 13 May 2011; revised 1 October 2011)

ABSTRACT

In this study, the impact of atmosphere–wave coupling on typhoon intensity was investigated using numerical simulations of an idealized typhoon in a coupled atmosphere–wave–ocean modeling system. The coupling between atmosphere and sea surface waves considered the effects of wave state and sea sprays on air–sea momentum flux, the atmospheric low-level dissipative heating, and the wave-state-affected sea-spray heat flux. Several experiments were conducted to examine the impacts of wave state, sea sprays, and dissipative heating on an idealized typhoon system. Results show that considering the wave state and sea-spray-affected sea-surface roughness reduces typhoon intensity, while including dissipative heating intensifies the typhoon system. Taking into account sea spray heat flux also strengthens the typhoon system with increasing maximum wind speed and significant wave height. The overall impact of atmosphere–wave coupling makes a positive contribution to the intensification of the idealized typhoon system. The minimum central pressure simulated by the coupled atmosphere–wave experiment was 16.4 hPa deeper than that of the control run, and the maximum wind speed and significant wave height increased by 31% and 4%, respectively. Meanwhile, within the area beneath the typhoon center, the average total upward air–sea heat flux increased by 22%, and the averaged latent heat flux increased more significantly by 31% compared to the uncoupled run.

Key words: wave state, sea spray, dissipative heating, tropical cyclone

Citation: Liu, B., C. L. Guan, L. A. Xie, and D. L. Zhao, 2012: An investigation of the effects of wave state and sea spray on an idealized typhoon using an air–sea coupled modeling system. *Adv. Atmos. Sci.*, **29**(2), 391–406, doi: 10.1007/s00376-011-1059-7.

1. Introduction

Air–sea momentum, heat, and moisture transfers are key processes in air–sea interaction, thus accurate estimation of these fluxes is essential to the coupled air–sea modeling system. A ubiquitous phenomenon at the sea surface, sea surface waves modify the current structure on both sides of air–sea interface, which in turn, can influence the air–sea exchanges of momentum and heat. Although the classical Charnock relation (Charnock, 1955), which implicitly includes surface wave effect, is widely used in atmospheric and surface wave models, it has been commonly recognized that wave state has an important impact on air–sea momentum flux (Toba et al., 1990; Donelan, 1990; Johnson et al., 1998; Drennan et al., 2003).

Since the early 1990s, due to improved understanding of wave-state effect on air–sea fluxes and the progress in high-performance computing, extensive coupled atmosphere–wave studies have been conducted to investigate the impacts of air–sea interactions on large-scale circulation (Weber et al., 1993; Janssen, 1994; Janssen and Viterbo, 1996; Weisse et al., 2000; Perrie and Zhang, 2001; Weisse and Schneggenburger, 2002), extratropical cyclones (Doyle, 1995; Lionello et al., 1998; Power and Stolinga, 2000; Desjardins et al., 2000; Lalbeharry et al., 2000), and tropical cyclones (Bao et al., 2000; Tenerelli et al.,

*Corresponding author: GUAN Changlong, clguan@ouc.edu.cn

2001; Doyle, 2002). Most previous studies utilized the wave-induced stress of Janssen (1989, 1991) or wave-age-dependent sea surface roughness (e.g., Smith et al., 1992; Donelan et al., 1993), in which younger waves correspond to larger surface roughness, to parameterize the air–sea momentum flux. However, based on field and laboratory observations, the Scientific Committee on Oceanic Research (SCOR) workgroup 101 (Jones and Toba, 2001) presented the SCOR relationship, showing that the non-dimensional sea-surface roughness first increases then decreases with increasing wave age. In addition, under high wind conditions, surface wave breaking and wind tearing wave crests disrupt the sea surface and produce sea sprays which might have a significant effect on sea-surface wind stress. Recent field and laboratory observations (Alamaro, 2001; Alamaro et al., 2002; Powell et al., 2003; Donelan et al., 2004) show that the drag coefficient does not increase but rather decreases with the increase of wind speed under high wind conditions due to sea foams and sea sprays.

The existence of sea spray droplets also has a significant impact on air–sea heat and moisture fluxes (e.g., Andreas et al., 1995). A number of studies have investigated the effect of sea spray on air–sea interaction and atmospheric systems by including sea spray heat fluxes in atmospheric models or coupled air–sea systems (Fairall et al., 1994; Kepert et al., 1999; Bao et al., 2000; Wang et al., 2001; Andreas and Emanuel, 2001; Li, 2004; Perrie et al., 2004; Zhang et al., 2006). However, these studies did not consider the effect of wave state on sea spray heat flux, though wave state has been reported to have significant effects on the sea spray generation function (SSGF) as well as on sea spray heat flux (Chaen, 1973; Iida et al., 1992; Piazzola et al., 2002; Zhao et al., 2006).

Under high wind conditions, dissipative heating can also have important effects on the atmosphere–wave system. Previous studies (Bister and Emanuel, 1998; Zhang and Altshuler, 1999; Businger and Businger, 2001) have shown that taking dissipative heating into account increases tropical cyclone intensity by 10%–20% as measured in maximum surface wind speed. Bister and Emanuel (1998) found that dissipative heating makes a positive contribution to tropical cyclone intensity and may increase the maximum surface wind speed by as much as 20%. Zhang and Altshuler (1999) found that the inclusion of dissipative heating increases hurricane intensity by 10% as measured in maximum surface wind speed. Because it depends on surface friction under the impact of wave state and sea sprays, dissipative heating should also be included in the coupled atmosphere–wave model, particularly concerning typhoon or hurricane systems.

Recently, by integrating the wave–current interaction model (Xie et al., 2001; Xie et al., 2008; Liu and Xie, 2009), and the atmosphere–wave interaction model (Liu, 2007; Liu et al., 2008), a coupled atmosphere–wave–ocean modeling system (CAWOMS) was established, which includes various atmosphere–wave, atmosphere–ocean, and wave–ocean coupling processes (Xie et al., 2010; Liu et al., 2011). Experiments on an idealized TC system using the CAWOMS show that the overall effects of atmosphere–wave–ocean coupling on TC intensity is determined by the balance between the oceanic negative feedback due to the TC-induced SST cooling and the overall wave-related positive feedback, which includes the impacts of wave state, dissipative heating, and sea sprays. However, details of the contribution of each factor among wave state, dissipative heating, and sea sprays to the overall wave-related positive feedback have not yet been examined.

In this study, we aimed to investigate the impacts of sea-state-dependent roughness, atmospheric dissipative heating, and sea-spray heat fluxes on an idealized typhoon system using the coupled modeling system and focusing mainly on atmosphere–wave coupling. Section 2 provides a description of the coupled modeling system. Section 3 describes the idealized typhoon case and the design of experiments, followed by simulation results in section 4. Finally, summary and conclusions are presented in section 5.

2. The air–sea coupled modeling system

The air–sea coupled modeling system utilized in this study is the CAWOMS (Liu et al., 2011), which consists of the Advanced Research Weather Research and Forecasting (WRF-ARW, referred to WRF hereafter) model (Skamarock et al., 2005), the Princeton Ocean Model (POM, Mellor and Blumberg, 1985), and the Simulating WAves Nearshore (SWAN) model (Booij et al., 1999). CAWOMS takes into account various wave-related effects, including wave state, sea-spray-affected sea-surface roughness, sea-spray heat fluxes, and dissipative heating in atmosphere-wave coupling. It also considers oceanic effects such as the feedback of SST cooling and the impact of sea surface current on wind stress in atmosphere–ocean coupling. Wave–ocean interactions, including radiation stress and wave-induced bottom stress, are also taken into account. These model components were coupled using the Model Coupling Toolkit (MCT, Jacob et al., 2005). A schematic illustration depicting the CAWOMS can be found in Liu et al. (2011). In this study, we mainly focused on the atmosphere–wave interaction, that is, the coupling between the atmospheric

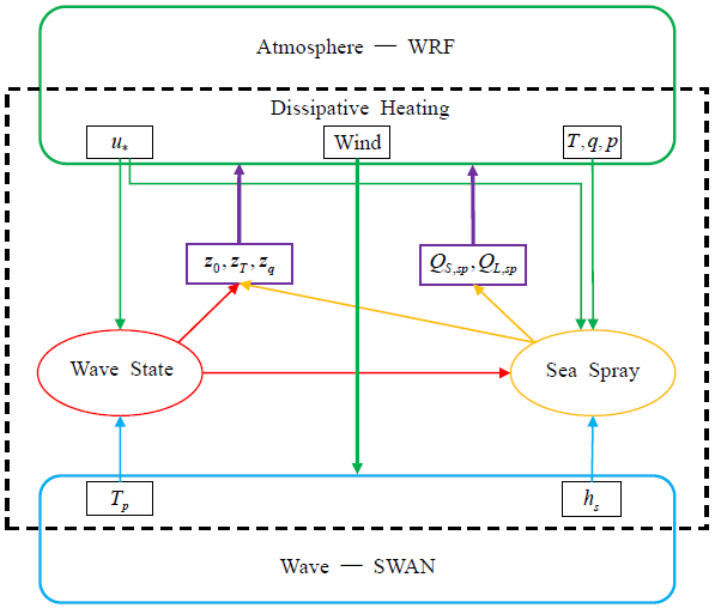

Fig. 1. Schematic of the atmosphere-wave coupling. u_* is friction velocity; T, q and p are atmospheric low level temperature, specific humidity, and pressure; z_0, z_r, and z_q are sea surface roughness parameters; $Q_{\mathrm{S,sp}}$ and $Q_{\mathrm{L,sp}}$ are sea spray sensible and latent heat fluxes; T_{p} is peak wave period; and h_{s} is significant wave height. The dashed square contains the various atmosphere-wave coupling processes.

WRF model and the SWAN wave model.

The WRF model was employed as the atmospheric model. It is a fully compressible, non-hydrostatic numerical weather prediction model suitable for a broad spectrum of applications across scales ranging from meters to thousands of kilometers. WRF utilizes an Arakawa-C grid with a terrain-following hydrostatic pressure coordinate system in the vertical. It provides multiple physics options for various physical processes, including microphysics, cumulus parameterization, planetary boundary layer (PBL), surface layer, land-surface, and long-wave and shortwave radiation. More details about the WRF model are provided on the WRF model website (http://www.wrf-model.org/index.php). The third-generation wave model, SWAN, was utilized as the sea-surface wave model. SWAN is based on an Eulerian formulation of the discrete spectral balance of action density that accounts for refractive propagation over arbitrary bathymetry and current fields. As in other third-generation wave models, the processes of wind wave generation, whitecapping, quadruplet wave–wave interactions, and bottom dissipation are taken into account. In addition, SWAN can consider the effects of triad wave interaction and depth-induced wave breaking for shallow-water waves.

The coupling between the atmospheric and wave model components is illustrated in Fig. 1, in which the dashed square contains the various atmosphere–wave coupling processes as well as the data exchanges of variables between the model components. WRF drives SWAN through sea surface wind U_{10}. It provides frictional velocity u_* for determining wave state (wave age β_* and wind–sea Reynolds number R_{B}); it also provides the atmospheric low-level environment variables such as temperature T, specific humidity q, surface pressure p, and frictional velocity u_* for estimating sea-spray heat fluxes. SWAN provides peak wave period T_{p} for determining wave state, and significant wave height h_{s} for estimating sea-spray heat fluxes. Wave state and sea sprays influence sea-surface roughness parameters (z_0, z_T, and z_q) and sea-spray heat fluxes ($Q_{\mathrm{S,sp}}$ and $Q_{\mathrm{L},sp}$), which in turn, impact the whole atmosphere–wave coupled system. In addition, atmospheric low-level dissipative heating is included in the WRF model. Details of the parameterization of the air–sea momentum and heat fluxes, the dissipative heating, and the estimation of sea-spray heat flux can be found in Xie et al. (2010) and Liu et al. (2011). They are briefly described here for convenience.

Conventionally, air–sea momentum flux is esti-

mated through the Charnock relation (Charnock, 1955):

$$gz_0/u_*^2 = \alpha\,, \tag{1}$$

where g is gravity, z_0 is the sea surface aerodynamic roughness, and α is the Charnock constant. In the WRF model, the Charnock constant was chosen as 0.0185 following Wu (1980), which was widely used in other atmospheric and wave models. The classical Charnock relation does not explicitly consider the wave-state effects on sea-surface roughness. During the past two decades, it has been commonly recognized that wave state has an important impact on air–sea momentum flux (Toba et al., 1990; Donelan, 1990; Johnson et al., 1998; Drennan et al., 2003). Recent studies (e.g., Alamaro et al., 2002; Powell et al., 2003; Donelan et al., 2004; Makin, 2005) also show that the classical Charnock relation is not applicable to high wind conditions. To consider both wave-state and sea-spray effects on sea-surface wind stress by combining the SCOR relation and the resistance law of Makin (2005), a parameterization of sea-surface aerodynamic roughness applicable to both low-to-moderate and high winds is obtained:

$$\alpha = \frac{gz_0}{u_*^2} = \begin{cases} (0.085\beta_*^{3/2})^{1-1/\omega}[0.03\beta_8\exp(-0.14\beta_*)]^{1/\omega}\,, & \sim 0.35 < \beta_* < 35 \\ 17.60^{1-1/\omega}(0.008)^{1/\omega}, & \beta_* \geqslant 35\,, \end{cases} \tag{2}$$

where $\beta_* = c_p/u_*$ is the wave age in which c_p is the phase speed at the peak of the wave spectrum, and $\omega = \min(1, a_{\rm cr}/\kappa u_*)$ is the correction parameter indicating the influence of sea spray on the logarithmic wind profile in which κ is the Karman constant and $a_{\rm cr}$=0.64 m s^{-1} is the critical value of terminal fall velocity of spray droplets (Makin, 2005). The roughness due to molecular viscosity $z_s = 0.11v/u_*$, where v is the kinematic molecular viscosity of air, is also added to sea-surface roughness (Smith, 1988).

For estimations of direct air–sea heat and moisture fluxes, the Coupled Ocean Atmosphere Response Experiment (COARE) algorithm V3.1 (Fairall et al., 2003) was adopted, in which the sea-surface scalar roughness parameters, z_T and z_q, are related to the Reynolds number of sea-surface aerodynamic roughness $Re_* = z_0u_*/v$ (with v being the kinematic molecular viscosity of air) through Eq. (3):

$$z_T = z_q = \min(1.1\times10^{-4}, 5.5\times10^{-5}Re^{-0.6})\,. \tag{3}$$

The dissipative heating in the lowest level of the atmospheric model is expressed as (Zhang and Altshuler, 1999)

$$\left.\frac{dT}{dt}\right|_{Dis} = \frac{V_{\rm a}u_*^2}{C_pz_1}\,, \tag{4}$$

where C_p is the air specific heat at constant pressure, z_1 is the height of model surface layer, and $V_{\rm a}$ is the wind speed at the model lowest semi-σ level. Dissipative heating is approximately proportional to the cubic power of surface wind speed, thus would be important under high winds, especially TC conditions. In the air–sea coupled modeling system, an equivalent upward heat flux $H_{\rm E} = \rho V_a u_*^2$ at the atmosphere surface layer is considered.

Another important issue to surface heat flux under high-wind conditions is the sea-spray heat flux. To estimate the sea-spray heat flux, we needed to know the sea-spray generation function (SSGF) dF/dr_0, quantifying how many sea-spray droplets of initial radius r_0 are produced per square meter of the surface per second per micrometer increment in droplet radius. As for the SSGF for spume droplets with radii generally >20 μm, based on field and laboratory observational data, Zhao et al. (2006) proposed a wave-state-dependent SSGF applicable to droplet radii between 30 μm and 500 μm. This SSGF depends on the wind–sea Reynolds number, $R_B = u_*^2/v\omega_p$, where u_*, v, and ω_p are friction velocity, molecular viscosity, and wave peak frequency, respectively. Wind–sea Reynolds number can also be expressed as $R_B = (gv)^{-1}u_*^3\beta_*$, and thereby is considered as a parameter combining the wind and wave-state effects. For bubble-derived droplets with radii typically <20 μm, introducing the whitecap coverage function of Zhao and Toba (2001) into the SSGF of Monahan (1986), a wind–sea Reynolds number (R_B) dependent on SSGF is obtained using

$$\begin{cases} \dfrac{dF}{dr_0} = 0.506R_B^{1.09}r_0^{-2.95}(1+0.029_{r_0}^{1.02})\times10^{1.19_{\exp(-B_0^2)}} \\ B_0 = (0.666 - 0.976\log r_0)/0.650\,. \end{cases} \tag{5}$$

Combining the SSGF applicable to bubble-derived droplets with the SSGF for spume droplets (Zhao et al., 2006), a wave-state-affected SSGF applicable to both bubble-derived droplet and spume droplet can be derived.

Concerning sea-spray droplet microphysics (Andreas, 1989; 1990), using Andreas (1992)'s method to estimate the "nominal" sea spray sensible and latent

Table 1. Comparison between the reality and the idealized settings for Typhoon Nabi (2005).

Reality of Nabi (2005)	Idealized settings
Real land-sea distribution	No Land
Real ocean with varying water depth	Ocean with constant water depth of 2500 m
Spatially and temporally varying SST	Constant SST of 29°C

heat fluxes (Q_S and Q_L), the total air–sea sensible and latent heat fluxes ($H_{S,T}$ and $H_{L,T}$) can be expressed as

$$\begin{cases} H_{S,T} = H_S + \beta Q_S - \alpha\gamma Q_L \\ H_{L,T} = H_L + \alpha Q_L \end{cases} \quad (6)$$

where α, β, and γ are non-negative feedback coefficients, H_S and H_L are the direct air–sea sensible and latent heat fluxes. The net sea-spray contribution to the total sensible and latent heat fluxes can then be estimated:

$$\begin{cases} Q_{S,sp} = \beta Q_S - \alpha\gamma Q_L \\ Q_{L,sp} = \alpha Q_L \end{cases} \quad (7)$$

Hereafter, $Q_{S,sp}$ and $Q_{L,sp}$ are called sea-spray sensible heat flux and sea-spray latent heat flux, respectively. α and γ are determined following Bao et al. (2000), while β is taken as 1 (Andreas, 1992). Equation (4), which includes the effect of wave state on sea-spray heat flux, was employed to estimate the net contribution of sea spray to air–sea sensible and latent heat fluxes in the air–sea coupled modeling system.

3. The idealized typhoon and experiment design

The idealized typhoon case in this study was based on the period from 0000 UTC 31 August to 0000 UTC 3 September 2005 of Typhoon Nabi (2005) over the western North Pacific basin. The model domain of the coupled system was centered at (22.5°N, 140.0°E) with the Mercator projection. It included 301×301 horizontal grid points, with grid spacing of 12 km. The model domain was assumed to be over open ocean, with a constant water depth of 2500 m. Thus, the effects of land–sea distribution and shallow water were neglected. The SST was set as 29°C and was kept constant during the model integration. Table 1 lists the comparison between the reality and the idealized settings used in this study for Typhoon Nabi (2005). The air–sea coupled modeling system exchanged variables between WRF and SWAN every 15 minutes, and the simulation results were saved every 3 h.

The WRF model has 30 full σ layers in the vertical direction from sea surface to 50 hPa with the lowest semi-σ layer at ∼21.5 m above sea surface. The integration time step was 60 seconds. The WSM5 microphysics scheme (Hong et al., 2004), Kain-Fritsch cumulus scheme (Kain and Fritsch, 1990), Yonsei University PBL scheme (Hong et al., 2006), as well as the Dudhia short wave (Dudhia, 1989) and rapid radiative transfer model (RRTM) long-wave (Mlawer et al., 1997) radiation scheme were chosen in the simulation of the idealized TC. Lateral boundary conditions were acquired from the NCEP GFS 1° analysis data. The model was initialized by a 12-h uncoupled WRF simulation (from 1200 UTC 30 August to 0000 UTC 31 August) with a bogus vortex implanted at 1200 UTC 30 August based on the typhoon intensity and location data from the Regional Specialized Meteorological Center (RSMC) Tokyo—Typhoon Center. The SWAN model resolves 32 frequencies logarithmically spaced from 0.0418 to 0.8023 Hz and 36 direction bands of 10° each. The time step was 15 minutes. The initial field was provided by the uncoupled 12-h SWAN simulation (from 1200 UTC 30 August to 0000 UTC 31 August), driven by the wind from the uncoupled WRF simulation.

To examine the impact of the atmosphere–wave coupling on the idealized typhoon system, four experiments were conducted. They were designed to evaluate the effects of wave state, sea spray, and dissipative heating on both atmospheric and sea-surface wave fields. Table 2 presents a summary of the experiments. Experiment CTRL was the control run, in which the atmospheric and wave model components were run in the same way as in the spin-up run. Wind fields from WRF were transferred to SWAN every 15 minutes, while no direct surface wave-related feedback effect on the atmospheric model was considered. The classical Charnock relation, Eq. (1), was used to parameterize the air–sea momentum flux. Neither the dissipative heating nor the sea-spray heat flux was taken into account. In experiment CPLZ0, WRF was coupled to SWAN only by considering the wave state and sea-

Table 2. Summary of the atmosphere-wave coupling for the experiments.

Expts.	Aerodynamic roughness	Dissipative heating	Sea spray heat flux
CTRL	Eq. (1)	No	No
CPLZ0	Eq. (2)	No	No
CPLZ0DH	Eq. (2)	Yes	No
CPLFULL	Eq. (2)	Yes	Yes

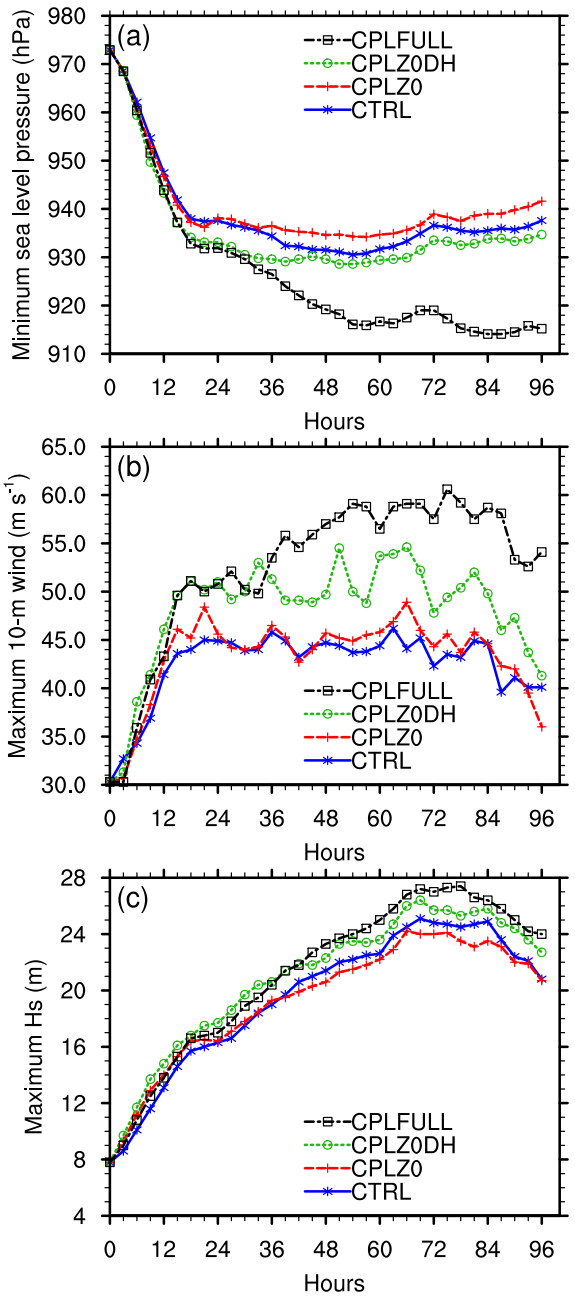

Fig. 2. Time series of the simulated minimum SLP (a), maximum 10-m wind speed (b) and maximum SWH (c) for each experiment.

spray-affected aerodynamic roughness as shown in Eq. (2). Compared to experiment CPLZ0, the CPLZ0DH experiment further considered the dissipative heating in the atmospheric surface layer, while experiment CPLFULL was the fully coupled experiment that included all of the effects of the wave state, sea spray, and dissipative heating. Based on the simulation results of these experiments, we examined the sensitivity of the coupled atmosphere–wave system to wave state, sea sprays, and dissipative heating. The results are presented in the following section, with emphases on their impacts on typhoon intensity, air–sea fluxes, as well as sea-surface waves.

Table 3. The simulated minimum central pressure, maximum 10-m wind, and maximum significant wave height of the idealized typhoon for each experiment.

Experiment	Min SLP (hPa)	Max U_{10} (m s^{-1})	Max H_s (m)
CTRL	930.5	46.2	25.1
CPLZ0	934.2	48.9	24.2
CPLZ0DH	928.6	54.6	26.4
CPLFULL	914.1	60.6	27.4

4. Results

4.1 *The impact of wave state and sea-spray-affected roughness*

Figure 2 shows the simulated time series of the min imum sea level pressure (SLP), the maximum 10-m wind speed, and the maximum significant wave height (SWH), respectively for experiments CTRL, CPLZ0, CPLZ0DH, and CPLFULL. The idealized typhoon quickly intensified within 24 h and reached its peak intensity at ∼56 h, though it reintensified during hours 72–84 in experiment CPLFULL. Table 3 lists the simulated minimum SLP, maximum 10-m wind, and maximum SWH of the idealized typhoon for each experiment. Comparing the simulated minimum SLP of experiment CPLZ0 to the result of the control run, the idealized typhoon was weakened by the increasing sea-surface roughness and surface friction due to wave-state effect. This result is consistent with previous coupled atmosphere–wave studies (e.g., Doyle, 1995; Lionello et al., 1998; Tenerelli et al., 2001). The minimum central pressure (934.2 hPa) of experiment CPLZ0 was 3.7 hPa higher than that of experiment CTRL (930.5 hPa). However, because the sea-spray effect reduces the drag coefficient and levels off the wind stress in areas with high winds, the maximum 10-m wind speed of experiment CPLZ0 was 48.9 m s^{-1}, corresponding to a 6% increase relative to the control run. Figures 3 and 4 show the simulated 54-h SLP and 10-m wind, the simulated 54-h SWH, and mean wave direction for each experiment, respectively. The strongest winds and waves were located in the northeast quadrant of the idealized typhoon. Comparing Fig. 3a to Fig. 3b, although the maximum wind speed of experiment CPLZ0 was slightly higher than that of experiment CTRL, the area with high winds (e.g., >30 m s^{-1}) for experiment CPLZ0 was much smaller than that for the control run. As a result, the simulated

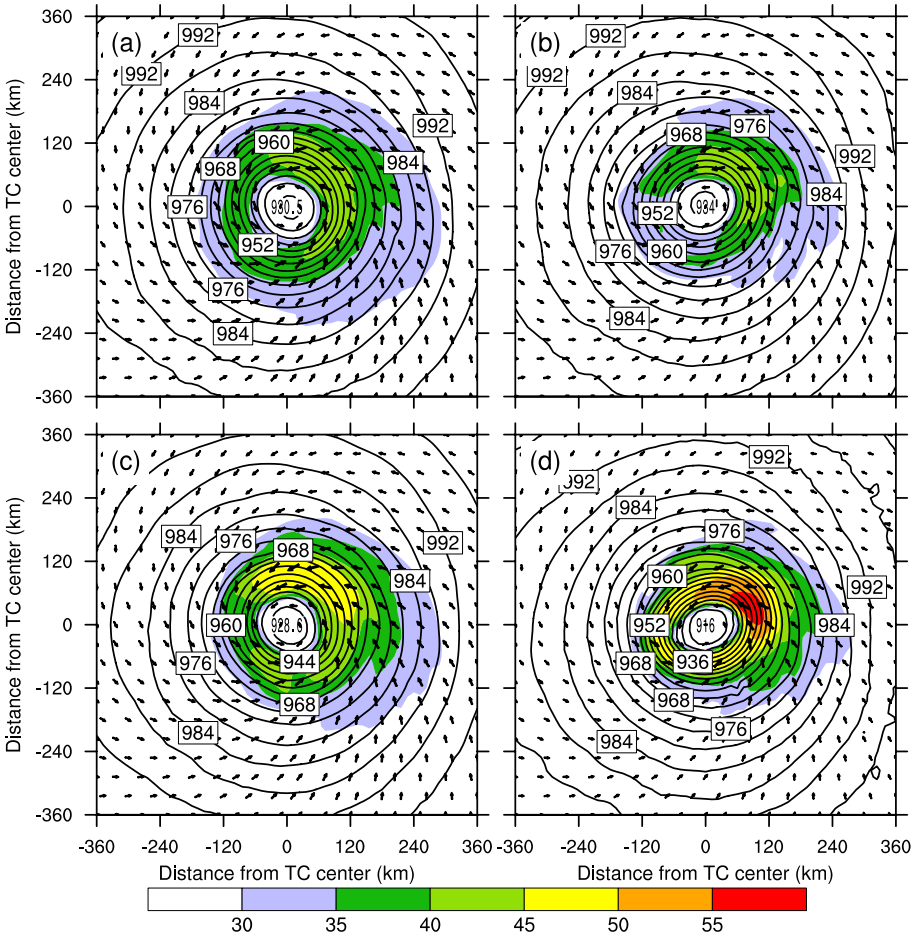

Fig. 3. The simulated 54-h SLP (contour every 4 hPa) and 10-m wind vector (arrows) and speed (shaded every 5 m s^{-1}) for experiments (a) CTRL, (b) CPLZ0, (c) CPLZ0DH, and (d) CPLFULL.

SWH for experiment CPLZ0 was smaller than that for experiment CTRL (Fig. 4), with the maximum SWH being reduced by 0.9 m (Table 4).

Figure 5 displays the simulated 54-h surface friction velocity, sea surface aerodynamic roughness, and wave age β_* for experiments CTRL and CPLZ0, respectively. The wave age distributions (bottom panels of Fig. 5) show that the wave age near the typhoon center was smaller than outside the center. As the control run uses the classical Charnock relation, which only considers the wind effect on surface roughness, the distribution patterns of friction velocity (Fig. 5a), and sea surface roughness (Fig. 5c) are similar to that of surface wind (Fig. 3a), with the maximum value located in the northeastern quadrant of the typhoon. Figure 6 shows the simulated 54-h relationships between the drag coefficient C_D and 10-m wind speed U_{10}, and between the Charnock parameter α and wave

Table 4. The simulated 54-h total sensible heat flux $H_{S,T}$, total latent heat flux $H_{L,T}$, direct sensible heat flux H_S, direct latent heat flux H_L, equivalent sensible heat flux to dissipative heating H_E, sea-spray sensible heat flux $Q_{S,sp}$, and sea-spray latent heat flux $Q_{L,sp}$ averaged over the 720×720 km^2 area centered at the typhoon eye for each experiment. (Units: W m^{-2}).

Experiment	$H_{S,T}$	$H_{L,T}$	H_S	H_L	H_E	$Q_{S,sp}$	$Q_{L,sp}$
CTRL	30.97	460.93	30.97	460.93	–	–	–
CPLZ0	30.26	466.01	30.26	466.01	–	–	–
CPLZ0DH	95.76	496.43	9.64	496.43	86.12	–	–
CPLFULL	−0.42	601.61	57.20	378.49	78.02	−135.63	223.12

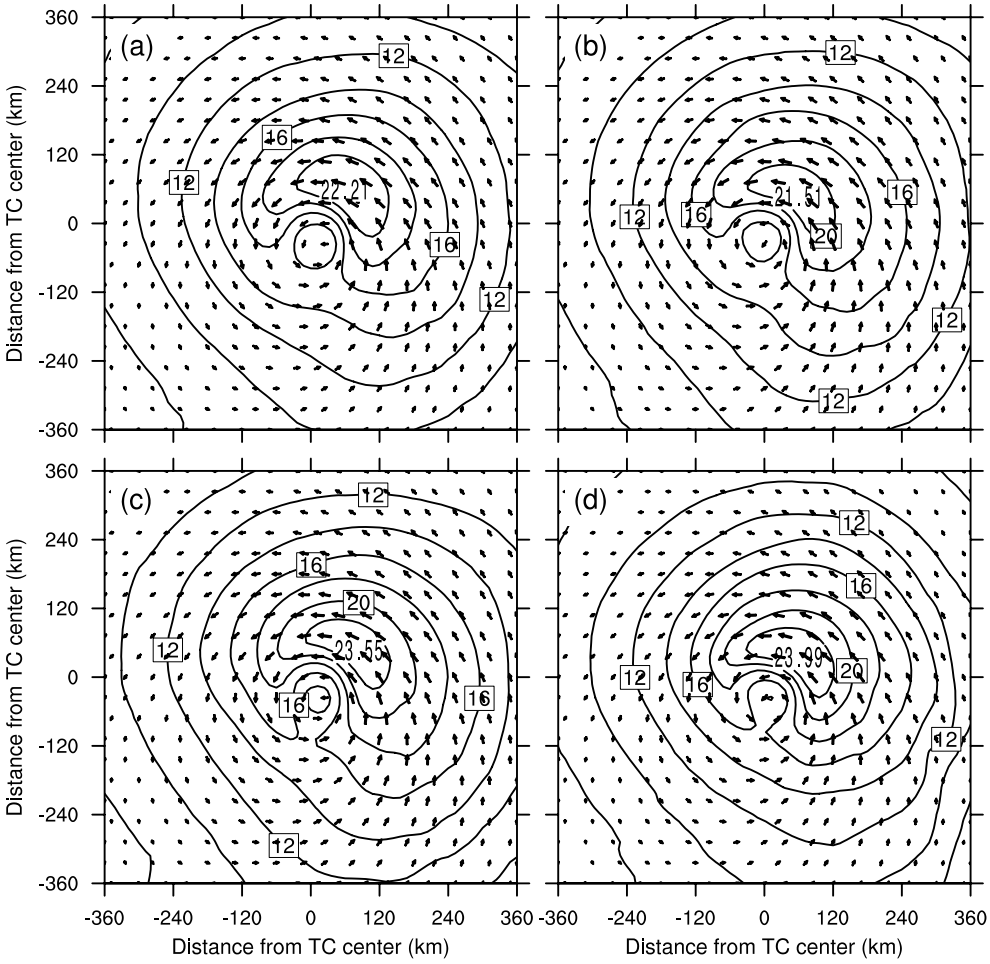

Fig. 4. The simulated 54-h SWH (contour every 2 m) and mean wave direction (arrows) for experiments (a) CTRL, (b) CPLZ0, (c) CPLZ0DH, and (d) CPLFULL.

age β_* for experiments CTRL and CPLZ0. The black points in the bottom panels correspond to 10-m wind speed <25 m s^{-1}, while the red "+" s correspond to 10-m wind speed >25 m s^{-1}. As shown in Figs. 6a and c, the simulated relation between Charnock parameter and wave age is consistent with the classical Charnock relation and the drag coefficient linearly increases with the wind speed. Considering the wave state and sea-spray-affected parameterization in experiment CPLZ0 led to the increase of surface roughness due to wave age effect under low-to-moderate winds and to the decrease of surface roughness due to sea-spray effect under high winds (Fig. 6b). Thus, the maximum sea-surface roughness was located in the southern section of the typhoon (Fig. 5d), where the wind speed was not extremely high and the wave age was relatively small. The simulated maximum sea-surface roughness in experiment CPLZ0 increased substantially relative to the control run. From the relation between the drag coefficient and wind speed simulated by experiment CPLZ0 (Fig. 6b), results show that the drag coefficient was no longer linearly dependent upon wind speed because of wave age effects, and the impact of sea sprays reduced the drag coefficient under high wind conditions. As shown in Fig. 6d, the Charnock parameter decreases with wave age, and the existence of sea spray under high winds significantly reduces the Charnock parameter.

Sea-surface scalar roughness parameters (z_T and z_q) depend upon the aerodynamic roughness Reynolds number as in Eq. (3). Therefore, wave state and sea spray can indirectly influence the air–sea sensible and latent heat fluxes through their impacts on aerodynamic roughness. In addition, the impacts of wave state and sea-spray-affected sea-surface roughness on typhoon intensity and surface wind can also modify air–sea heat and moisture fluxes. Figure 7 illustrates the simulated 54-h upward sensible and latent heat fluxes for experiments CTRL and CPLZ0. The simulated sensible and latent heat fluxes for experiments

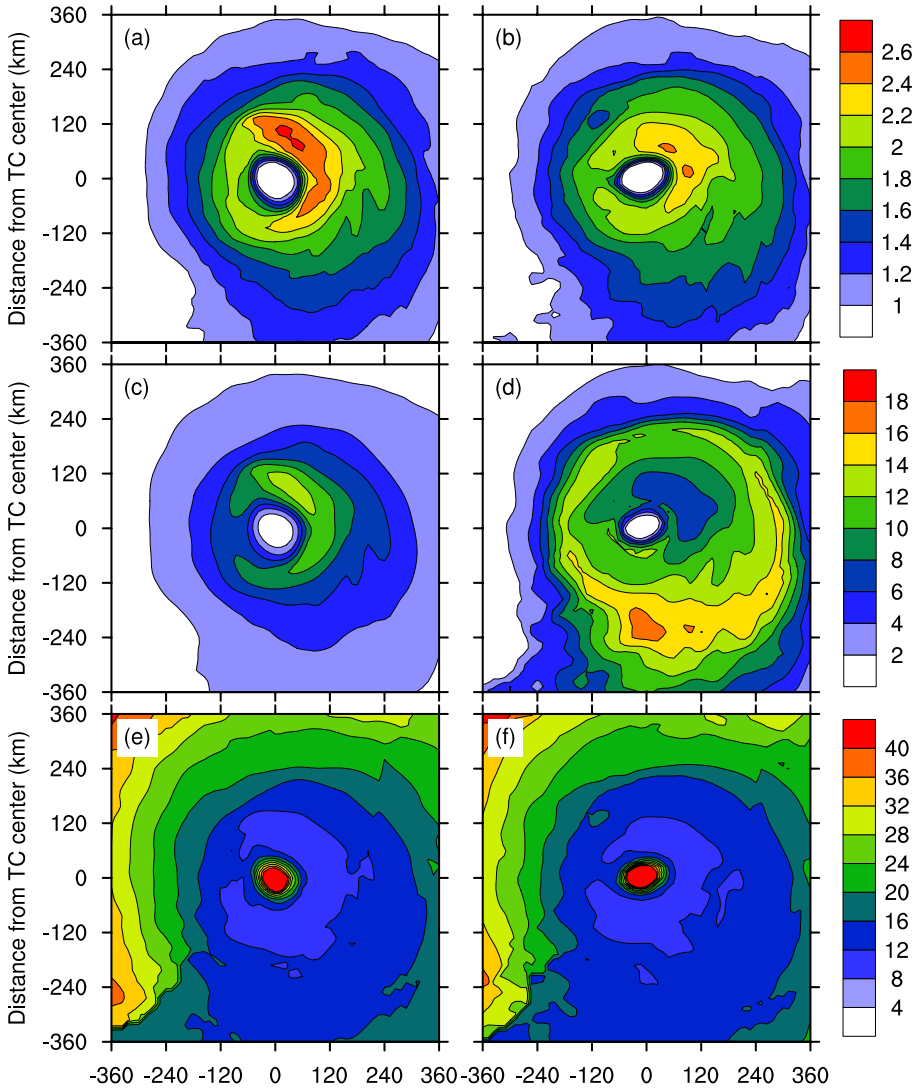

Fig. 5. The simulated 54-h (top) friction velocity (in m s^{-1}), (middle) sea surface aerodynamic roughness (in 10^{-3} m), and (bottom) wave age β_* for experiments (left) CTRL and (right) CPLZ0.

CTRL and CPLZ0 have similar patterns, with a somewhat larger upward heat fluxes in the control run due to larger surface wind in experiment CTRL (Fig. 3).

Table 4 lists the simulated 54-h total sensible heat flux $H_{S,T}$, total latent heat flux $H_{L,T}$, direct sensible heat flux H_S, direct latent heat flux H_L, equivalent sensible heat flux to dissipative heating H_E, sea-spray sensible heat flux $Q_{S,sp}$, and sea-spray latent heat flux $Q_{L,sp}$, averaged over the 720×720 km^2 area centered at the typhoon eye for each experiment. Comparing the results for experiment CPLZ0 with those for the control run, the averaged sensible and latent heat fluxes changed only a little when the wave state and sea-spray effects on sea surface roughness were considered; the total upward heat flux increased by <1%.

4.2 *The impact of dissipative heating*

The impact of dissipative heating on a typhoon system is complicated. It includes both positive and negative feedback processes. On one hand, dissipative heating in the atmospheric lower level is equivalent to an additional upward sensible heat flux, increasing the total upward heat flux and intensifying the typhoon system. On the other hand, the increase in sensible heat flux increased low-level air temperature and thus reduced air–sea temperature difference, which in turn, reduces the air–sea direct sensible heat flux.

As shown in Fig. 2 and Table 3, comparing the results of experiment CPLZ0DH to those of experiment CPLZ0, the minimum SLP simulated by experiment CPLZ0DH is 5.6 hPa deeper than that from experi-

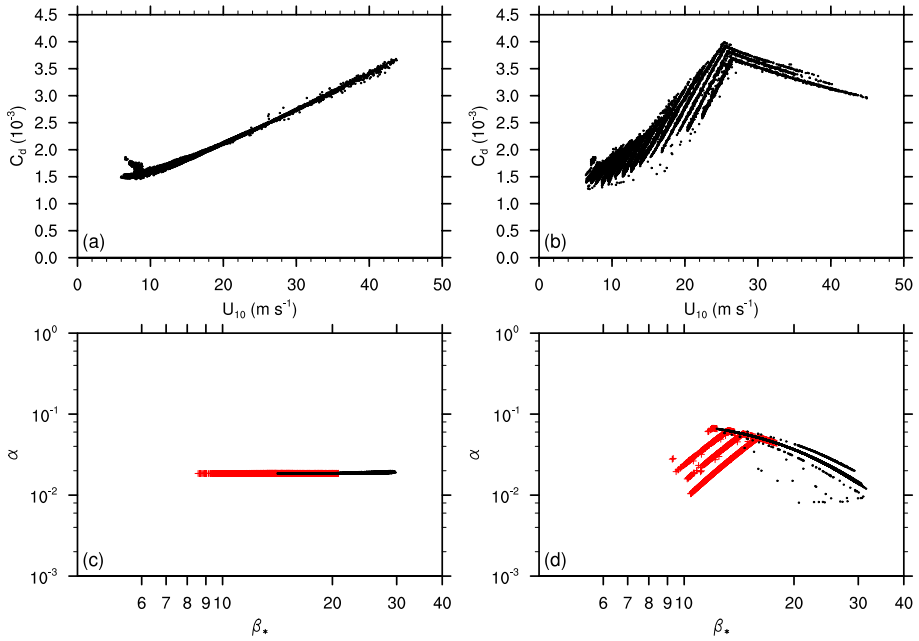

Fig. 6. The simulated 54-h (top) relation between the drag coefficient C_D and 10-m wind speed U_{10}, and (bottom) relation between the Charnock parameter α and wave age β_* for experiments (left) CTRL and (right) CPLZ0. The black points in the bottom panels correspond to 10-m wind speed less than 25 m s^{-1}, while the red "+"s correspond to 10-m wind speed larger than 25 m s^{-1}.

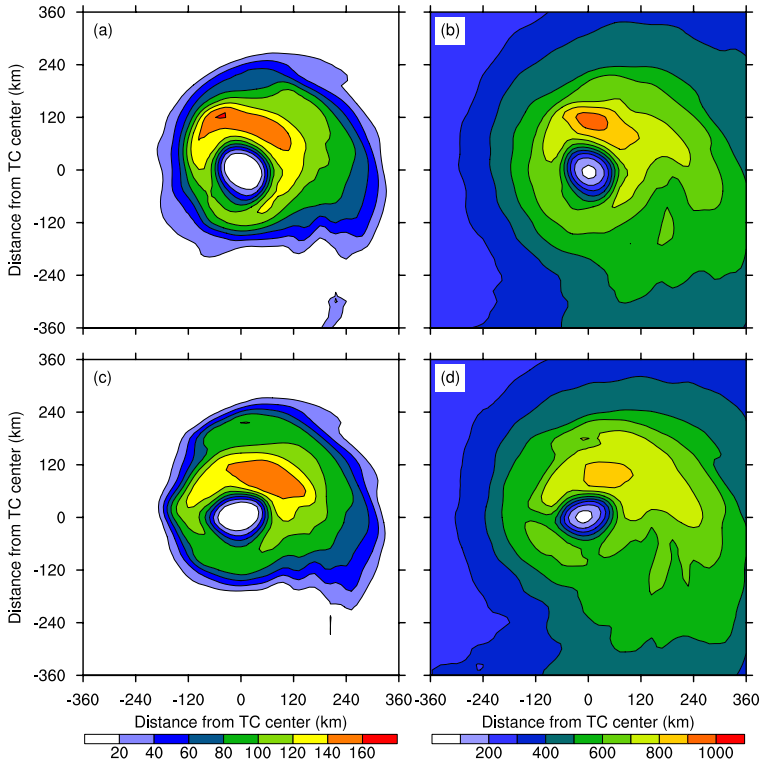

Fig. 7. The simulated 54-h upward (left) sensible heat flux and (right) latent heat flux for experiments (top) CTRL and (bottom) CPLZ0. (Units: W m^{-2})

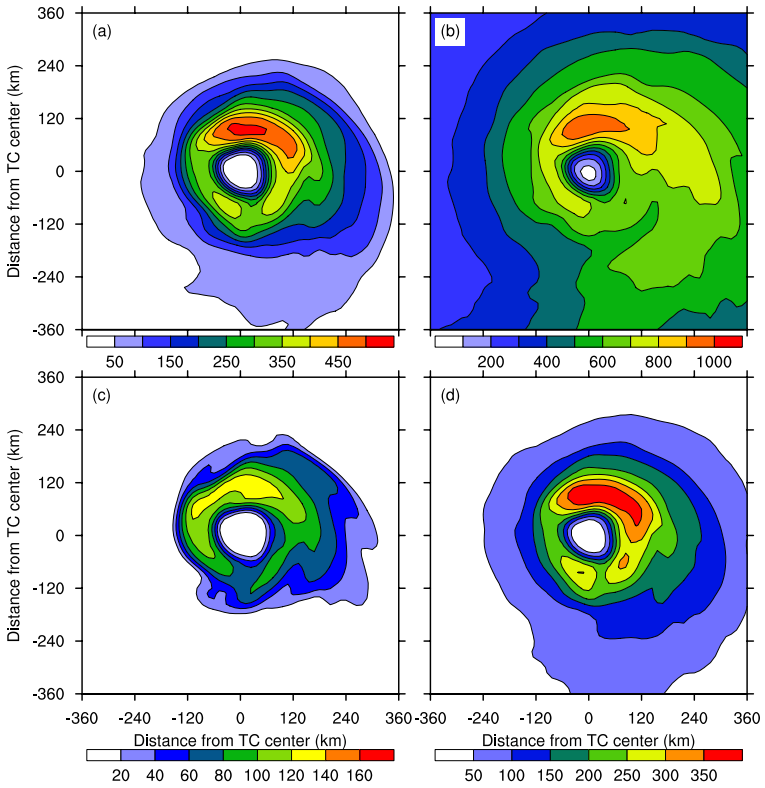

Fig. 8. The simulated 54-h (a) total sensible heat flux $H_{S,T}$, (b) total latent heat flux $H_{L,T}$, (c) direct sensible heat flux H_S, and (d) equivalent sensible heat flux to dissipative heating H_E for experiment CPLZ0DH. (Units: W m^{-2})

ment CPLZ0. The maximum 10-m wind speed and the maximum SWH also increased by 12% and 9%, respectively. Thus, the net contribution of considering dissipative heating in atmosphere–wave coupling to the intensity of the idealized typhoon system was positive. These results agree with those of previous studies (e.g., Bister and Emanuel, 1998; Zhang and Altshuler, 1999). Meanwhile, taking into account both wave state and sea-spray-affected sea-surface roughness and dissipative heating makes the simulated minimum SLP 1.9 hPa deeper in the CPLZ0DH run than in the CTRL run, with an 18% increase in the maximum wind speed, and a 5% increase in the maximum SWH.

Figure 8 shows the simulated 54-h total sensible heat flux $H_{S,T}$, total latent heat flux $H_{L,T}$, direct sensible heat flux H_S, and equivalent sensible heat flux to dissipative heating H_E for experiment CPLZ0DH. Due to the cubic power dependence on wind speed, dissipative heating was negligible in low-wind areas but was significant in high-wind areas (Fig. 8d). Dissipative heating can be larger than two times of the direct sensible heat flux in a high-wind region. A comparison between the results of experiments CPLZ0 (Fig. 8) and CTRL (Fig. 7) shows that taking into account dissipative heating reduces direct sensible heat flux, while it enhances latent heat flux. As shown in Table 4, which lists the averaged heat fluxes over the 720×720 km^2 area underneath the typhoon, the simulated total sensible heat flux for experiment CPLZ0DH increased significantly from 30.97 W m^{-2} for experiment CTRL and 30.26 W m^{-2} for experiment CPLZ0 to 95.76 W m^{-2}. And the simulated total latent heat flux for experiment CPLZ0DH increased by about 8% relative to the control run, leading to a 20% increase of the total upward heat flux.

4.3 *The impact of sea spray heat flux*

As shown in Fig. 2 and Table 3, the fully coupled atmosphere–wave coupled experiment CPLFULL reached the lowest minimum SLP (914.1 hPa), which was 20.1 hPa deeper than experiment CPLZ0 and 16.4 hPa deeper than the control run. The maximum 10-m wind speed simulated by experiment CPLFULL was 60.6 m s^{-1}, which was 24% and 31% stronger than those of experiments CPLZ0 and CTRL, respectively. The maximum SWH simulated by experiment CPLFULL also increased by 13% and 9% relative to experiments CPLZ0 and CTRL, respectively. The re-

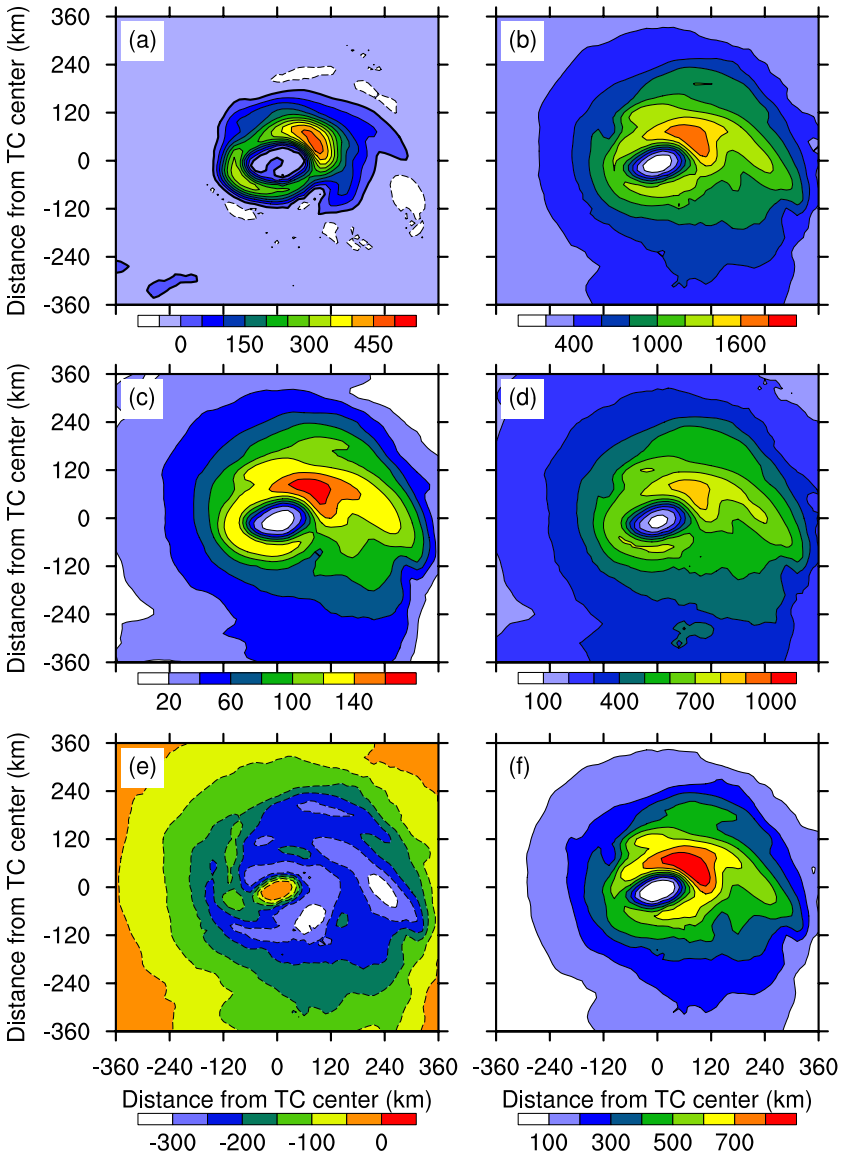

Fig. 9. The simulated 54-h (a) total sensible heat flux $H_{S,T}$, (b) total latent heat flux $H_{L,T}$, (c) direct sensible heat flux H_S, (d) direct latent heat flux H_L, (e) sea spray sensible heat flux $Q_{S,sp}$, and (f) sea spray latent heat flux $Q_{L,sp}$ for experiment CPLFULL. (Units: W m^{-2})

sults also show that the simulated minimum SLP for experiment CPLFULL was 14.5 deeper than that for experiment CPLZ0DH, with the maximum 10-m wind and SWH increasing by 11% and 4%, respectively.

Figure 9 shows the 54-h total sensible heat flux $H_{S,T}$, total latent heat flux $H_{L,T}$, direct sensible heat flux H_S, direct latent heat flux H_L, sea-spray sensible heat flux $Q_{S,sp}$, and sea-spray latent heat flux $Q_{L,sp}$ simulated by experiment CPLFULL. In this figure, the sea-spray sensible and latent heat fluxes are significant in areas with strong winds and waves. The sea-spray sensible heat flux is negative; thus it made a negative contribution to the total upward sensible heat flux; whereas, the sea spray latent heat flux made a positive contribution to the total latent heat flux. These results are similar to those of Fairall et al. (1994) and Kepert et al. (1999). Compared with experiments CTRL and CPLZ0, the impact of sea-spray heat flux increased the direct sensible heat flux but decreased the direct latent heat flux. This is because the evaporation of the spray droplets reduced low-level air temperature and increased low-level moisture, which in turn, increased air–sea temperature difference and reduced the air–sea moisture difference. Figure 10 shows the 54-h dissipa-

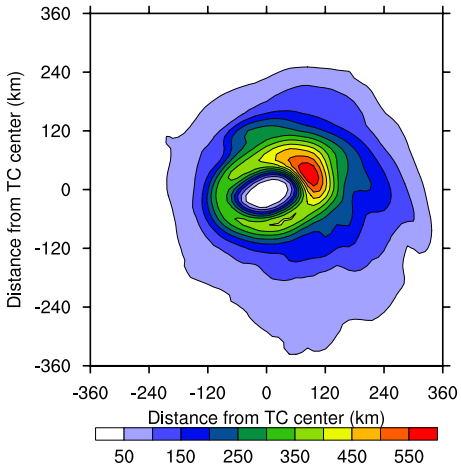

Fig. 10. The simulated 54-h equivalent sensible heat flux to dissipative heating $H_{\rm E}$ (in W m^{-2}) for experiment CPLFULL.

tive heating $H_{\rm E}$ simulated by experiment CPLFULL. Its distribution was similar to that of experiment CPLZ0DH; however, the maximum value was larger because of the increased surface wind speed. From Table 4, one can find that the total heat flux simulated by CPLFULL showed an increase of 22% relative to the control run, with the latent heat flux being increased by 31%.

In these analyses, we examined the impacts of sea state, dissipative heating and sea spray on the intensity of the idealized typhoon. However, their effects on typhoon track are negligible because the track is generally determined by the large-scale environmental flow. The simulated tracks by all four experiments show no significant differences (figure not shown here). Notably, the impacts of wave state, sea spray and dissipative heating are not isolated. Wave state and sea spray influence surface wind stress, thus impacting the dissipative heating; while the effect of dissipative heating intensifies the typhoon system, changes sea-surface wind, and leads to an influence on surface wave parameters. Wave state can also affect the sea-spray generation and sea-spray heat fluxes, which influence the intensity of the typhoon system; the modified surface wind field thus changes the surface wave field and sea state. In addition, the atmospheric surface layer dissipative heating affords more heat for the evaporation of spray droplets, while the influence of sea spray heat flux will change surface wind and dissipative heating.

5. Conclusions

Using a coupled atmosphere–wave–ocean modeling system, the impact of atmosphere–wave coupling on an idealized typhoon was investigated. In the air–sea coupled modeling system, the parameterization of wave state, and sea-spray effects on sea-surface roughness applicable to wind conditions ranging from low to high wind speeds was adopted to estimate the air–sea momentum flux. The atmospheric dissipative heating and the wave-state influenced sea-spray heat flux, which made significant contributions to air–sea heat fluxes under high winds, were also taken into account in the atmosphere–wave coupling processes.

Several experiments were conducted for an idealized typhoon system to investigate the impacts of wave state and sea spray affected roughness, dissipative heating, and sea-spray heat flux on the intensity of the typhoon system. Using the wave state and sea-spray-affected sea-surface roughness instead of the classical Charnock relation, the typhoon system was weakened by the increase of surface roughness, with shallower minimum SLP and smaller maximum SWH. Meanwhile, the maximum surface wind increased due to the reduction of drag coefficient when considering the impact of sea sprays in high wind areas. The inclusion of dissipative heating, which depends on surface friction increases the air–sea heat flux and intensifies the typhoon system. Incorporating the wave-state-dependent sea-spray heat flux also strengthened the typhoon system. The sea-spray heat flux along with the feedback effect to the environment significantly changed the proportion of sensible heat flux and latent heat flux by reducing the sensible heat flux while increasing the latent heat flux, which in turn, enhanced the typhoon intensity and increased surface wind speed as well as wave height.

Notably, the impacts of wave state and sea-spray-affected sea-surface roughness, dissipative heating, and sea-spray heat flux interacted with each other through air–sea interaction processes. When all three impacts were considered, the minimum SLP in the fully coupled atmosphere–wave coupled experiment was 16.4 hPa deeper than that in the uncoupled run, with the maximum wind speed and SWH being increased by 31% and 4%, respectively. The averaged total air–sea heat flux over the 720×720 km^2 area underneath the typhoon increased by ∼22%, while the latent heat flux increased more significantly (by 31%), compared to the control run.

Acknowledgements. The authors are grateful for the English proofreading by Ms. Katie Costa and Prof. Jamie Larsen. This study was supported by the National Natural Science Foundation of China (Grant Nos. 40830959, 40921004 and 41076007), the Ministry of Science and Technology of China (Grant No. 2011BAC03B01), and the U.S. National Science Foundation (Grant No. AGS1043125).

REFERENCES

Alamaro, M., 2001: Wind wave tank for experimental investigation of momentum and enthalpy transfer from the ocean surface at high wind speed. M. S. thesis, Department of Earth, Atmospheric and Planetary Sciences, Massachusetts Institute of Technology, 79pp.

Alamaro, M., K. A. Emanuel, J. J. Colton, W. R. McGillis, and J. Edson, 2002: Experimental investigation of air-sea transfer of momentum and enthalpy at high wind speed. *25th Conference on Hurricanes and Tropical Meteorology*, San Diego, CA, Amer. Meteor. Soc., 17C.6. [Available online at http://ams.confex.com/ams/25HURR/techprogram/paper_35185.htm].

Andreas, E. L., 1989: Thermal and size evolution of sea spray droplets. CRREL Rep. 89-11, 47pp. [Available online at http://oai.dtic.mil/oai/oai?verb=getRecord&metadataPrefix=html&identifier=ADA210484].

Andreas, E. L., 1990: Time constants for the evolution of sea spray droplets. *Tellus* (*B*), **42**, 481–497.

Andreas, E. L., 1992: Sea spray and the turbulent air-sea heat fluxes. *J. Geophys. Res.*, **97**, 11429–11441.

Andreas, E. L., and K. A. Emanuel, 2001: Effects of sea spray on tropical cyclone intensity. *J. Atmos. Sci.*, **58**, 3741–3751.

Andreas, E. L., J. B. Edson, E. C. Monahan, M. P. Rouault, and S. D. Smith, 1995: The spray contribution to net evaporation from the sea: A review of recent progress. *Bound.-Layer Meteor.*, **72**, 3–52.

Bao, J.-W., J. M. Wilczak, J.-K. Choi, and L. H. Kantha, 2000: Numerical simulations of air-sea interaction under high wind conditions using a coupled model: A study of hurricane development. *Mon. Wea. Rev.*, **128**, 2190–2210.

Bister, M., and K. A. Emanuel, 1998: Dissipative heating and hurricane intensity. *Meteor. Atmos. Phys.*, **65**, 233–240.

Booij, N., R. C. Ris, and L. H. Holthuijsen, 1999: A third-generation wave model for coastal regions, 1. Model description and validation. *J. Geophys. Res.*, **104**, 7649–7666.

Businger, S., and J. A. Businger, 2001: Viscous dissipation of turbulence kinetic energy in storms. *J. Atmos. Sci.*, **58**, 3793–3796.

Chaen, M., 1973: Studies on the production of sea-salt particles on the sea surface. *Memoirs of the Faculty of Fisheries, Kagoshima University*, **22**, 49–107.

Charnock, H., 1955: Wind stress on a water surface. *Quart. J. Roy. Meteor. Soc.*, **81**, 639–640.

Desjardins, S., J. Mailhot, and R. Lalbeharry, 2000: Examination of the impact of a coupled atmospheric and ocean wave system. Part I: Atmospheric aspects. *J. Phys. Oceanogr.*, **30**, 385–401.

Donelan, M. A., 1990: Air-sea interaction. *The Sea: Ocean Engineering Science*, Mehaute and Hanes, Eds., Wiley-Interscience, 239–292.

Donelan, M. A., F. W. Dobson, S. D. Smith, and R. J. Anderson, 1993: On the dependence of sea surface roughness on wave development. *J. Phys. Oceanogr.*, **23**, 2143–2149.

Donelan, M. A., and Coauthors, 2004: On the limiting aerodynamic roughness of the ocean in very strong winds. *Geophys. Res. Lett.*, **31**, L18306, doi: 18310.11029/12004GL019460.

Doyle, J. D., 1995: Coupled ocean wave/atmosphere mesoscale model simulations of cyclogenesis. *Tellus*, **47A**, 766–788.

Doyle, J. D., 2002: Coupled atmosphere-ocean wave simulations under high wind conditions. *Mon. Wea. Rev.*, **130**, 3087–3099.

Drennan, W. M., H. C. Graber, D. Hauser, and C. Quentin, 2003: On the wave age dependence of wind stress over pure wind seas. *J. Geophys. Res.*, **108**, 8062, doi: 8010.1029/2000JC000715.

Dudhia, J., 1989: Numerical study of convection observed during the winter monsoon experiment using a mesoscale two-dimensional model. *J. Atmos. Sci.*, **46**, 3077–3107.

Fairall, C. W., J. D. Kepert, and G. J. Holland, 1994: The effect of sea spray on surface energy transports over the ocean. *The Global Atmosphere-Ocean System*, **2**, 121–142.

Fairall, C. W., E. F. Bradley, J. E. Hare, A. A. Grachev, and J. B. Edson, 2003: Bulk parameterization of air-sea fluxes: Updates and verification for the COARE algorithm. *J. Climate*, **16**, 571–591.

Hong, S.-Y., J. Dudhia, and S.-H. Chen, 2004: A revised approach to ice microphysical processes for the bulk parameterization of clouds and precipitation. *Mon. Wea. Rev.*, **132**, 103–120.

Hong, S.-Y., Y. Noh, and J. Dudhia, 2006: A new vertical diffusion package with an explicit treatment of entrainment processes. *Mon. Wea. Rev.*, **134**, 2318–2341.

Iida, N., Y. Toba, and M. Chaen, 1992: A new expression for the production rate of sea water droplets on the sea surface. *J. Oceanogr.*, **48**, 439–460.

Jacob, R., J. Larson, and E. Ong, 2005: $M \times N$ communication and parallel interpolation in Community Climate System Model Version 3 using the model coupling toolkit. *International Journal of High Performance Computing Applications*, **19**, 293–307.

Janssen, P. A. E. M., 1989: Wave-induced stress and the drag of airflow over sea waves. *J. Phys. Oceanogr.*, **19**, 745–754.

Janssen, P. A. E. M., 1991: Quasi-linear theory of wind-wave generation applied to wave forecasting. *J. Phys. Oceanogr.*, **21**, 1631–1642.

Janssen, P. A. E. M., 1994: Results with a coupled wind wave model. ECMWF Tech. Rep. No. 71, 58pp.

Janssen, P. A. E. M., and P. Viterbo, 1996: Ocean waves and the atmospheric climate. *J. Climate*, **9**, 1296–1287.

Johnson, H. K., J. Hojstrup, H. J. Vested, and S. E. Larsen, 1998: On the Dependence of Sea Surface

Roughness on Wind Waves. *J. Phys. Oceanogr.*, **28**, 1702–1716.

Jones, I. S. F., and Y. Toba, 2001: *Wind Stress over the Ocean.* Cambridge University Press, 307pp.

Kain, J. S., and J. M. Fritsch, 1990: A one-dimensional entraining/detraining plume model and its application in convective parameterization. *J. Atmos. Sci.*, **47**, 2784–2802.

Kepert, J. D., C. W. Fairall, and J.-W. Bao, 1999: *Modelling the Interaction between the Atmospheric Boundary Layer and Evaporating Sea Spray Droplets.* Kluwer Academic Publishers, 363–409.

Lalbeharry, R., J. Mailhot, S. Desjardins, and L. Wilson, 2000: Examination of the impact of a coupled atmospheric and ocean wave system. Part II: Ocean wave aspects. *J. Phys. Oceanogr.*, **30**, 402–415.

Li, W., 2004: Modelling air-sea fluxes during a western Pacific typhoon: Role of sea spray. *Adv. Atmos. Sci.*, **21**, 269–276.

Lionello, P., P. Malguzzi, and A. Buzzi, 1998: On the coupling between the atmospheric circulation and the ocean wave field: An idealized case. *J. Phys. Oceanogr.*, **28**, 161–177.

Liu, B., 2007: Physical basis and numerical study of the coupled atmosphere-wave model. Ph.D. dissertation, Ocean University of China, 156pp.

Liu, B., C. Guan, and L. Xie, 2008: Investigating the impacts of wave state and sea spray on typhoon via a coupled atmosphere-wave system: The idealized case. *28th Conference on Hurricanes and Tropical Meteorology*, Orlando, Florida, American Meteorological Society. [Available online at http://ams.confex.com/ams/pdfpapers/138367.pdf].

Liu, B., H. Liu, L. Xie, C. Guan, and D. Zhao, 2011: A coupled atmosphere–wave–ocean modeling system: Simulation of the intensity of an idealized tropical cyclone. *Mon. Wea. Rev.*, **139**, 132–152.

Liu, H., and L. Xie, 2009: A numerical study on the effects of wave-current-surge interactions on the height and propagation of sea surface waves in Charleston Harbor during Hurricane Hugo 1989. *Continental Shelf Research*, **29**, 1454–1463.

Makin, V. K., 2005: A note on the drag of the sea surface at hurricane winds. *Bound.-Layer Meteor.*, **115**, 169–176.

Mellor, G. L., and A. F. Blumberg, 1985: Modeling vertical and horizontal diffusivities with the sigma coordinate system. *Mon. Wea. Rev.*, **113**, 1379–1383.

Mlawer, E. J., S. J. Taubman, P. D. Brown, M. J. Iacono, and S. A. Clough, 1997: Radiative transfer for inhomogeneous atmosphere: RRTM, a validated correlated-k model for the longwave. *J. Geophys. Res.*, **102**, 16663–16682.

Monahan, E. C., 1986: The ocean as a source for atmospheric particles. *The Role of Air-Sea Exchange in Geochemical Cycling*, Buat-Menard, Ed., D. Reidel Publishing Company, Dordrecht, 129–163.

Perrie, W., and Y. Zhang, 2001: A regional climate model coupled to ocean waves: Synoptic to multimonthly simulations. *J. Geophys. Res.*, **106**, 17753–17771.

Perrie, W., W. Zhang, X. Ren, Z. Long, E. L. Andreas, J. Gyakum, and R. McTaggart-Cowan, 2004: The role of waves, sea spray and the upper ocean in midlatitude storm development. Preprints, *26th Conference on Hurricanes and Tropical Meteorology of the American Meteorological Society*, Miami, FL, 2pp.

Piazzola, J., P. Forget, and S. Despiau, 2002: A sea spray generation function for fetch-limited conditions. *Ann. Geophys.*, **20**, 121–131.

Powell, M. D., P. J. Vickery, and T. A. Reinhold, 2003: Reduced drag coefficient for high wind speeds in tropical cyclones. *Nature*, **422**, 279–283.

Powers, J. G., and M. T. Stoelinga, 2000: A coupled air-sea mesoscale model: Experiments in atmospheric sensitivity to marine roughness. *Mon. Wea. Rev.*, **128**, 208–228.

Skamarock, W. C., J. B. Klemp, J. Dudhia, D. O. Gill, D. M. Barker, W. Wang, and J. G. Powers, 2005: A description of the Advanced Research WRF Version 2. NCAR Technical Note NCAR/TN-468+STR, 88pp.

Smith, S. D., 1988: Coefficients for sea surface wind stress, heat flux, and wind profiles as a function of wind speed and temperature. *J. Geophys. Res.*, **93**, 15467–15472.

Smith, S. D., and Coauthors, 1992: Sea surface wind stress and drag coefficients: The HEXOS results. *Bound.-Layer Meteor.*, **60**, 109–142.

Tenerelli, J. E., S. S. Chen, W. Zhao, and M. A. Donelan, 2001: High-resolution simulations of hurricane Floyd using MM5 coupled with a wave model. *Workshop Program for the Eleventh PSU/NCAR MM5 Users' Workshop*, 4pp.

Toba, Y., N. Iida, H. Kawamura, N. Ebuchi, and I. S. F. Jones, 1990: The wave dependence of sea-surface wind stress. *J. Phys. Oceanogr.*, **20**, 705–721.

Wang, Y., J. D. Kepert, and G. J. Holland, 2001: The effect of sea spray evaporation on tropical cyclone boundary layer structure and intensity. *Mon. Wea. Rev.*, **129**, 2481–2500.

Weber, S. L., H. V. Storch, P. Viterbo, and L. Zambresky, 1993: Coupling an ocean wave model to an atmospheric general circulation model. *Climate Dyn.*, **9**, 53–61.

Weisse, R., and C. Schneggenburger, 2002: The effect of different sea state dependent roughness parameterizations on the sensitivity of the atmospheric circulation in a regional model. *Mon. Wea. Rev.*, **130**, 1595–1602.

Weisse, R., H. Heyen, and H. Von Storch, 2000: Sensitivity of a regional atmospheric model to a sea state-dependent roughness and the need for ensemble calculations. *Mon. Wea. Rev.*, **128**, 3631–3642.

Wu, J., 1980: Wind-stress coefficients over sea surface near neutral conditions—A revisit. *J. Phys. Oceanogr.*, **13**, 1441–1451.

Xie, L., H. Liu, and M. Peng, 2008: The effect of wave-current interactions on the storm surge and inundation in Charleston Harbor during Hurricane Hugo

1989. *Ocean Modelling*, **20**, 252–269.

Xie, L., K. Wu, L. Pietrafesa, and C. Zhang, 2001: A numerical study of wave-current interaction through surface and bottom stresses: Wind-driven circulation in the South Atlantic Bight under uniform winds. *J. Geophys. Res.*, **106**, 16841–16855.

Xie, L., B. Liu, H. Liu, and C. Guan, 2010: Numerical simulation of tropical cyclone intensity using an air-sea-wave coupled prediction system. *Advances in Geosciences*, **18**(OS), 19–43.

Zhang, D.-L., and E. Altshuler, 1999: The effects of dissipative heating on hurricane intensity. *Mon. Wea. Rev.*, **127**, 3032–3038.

Zhang, W., W. Perrie, and W. Li, 2006: Impacts of waves and sea Sspray on midlatitude storm structure and intensity. *Mon. Wea. Rev.*, **134**, 2418–2442.

Zhao, D., and Y. Toba, 2001: Dependence of whitecap coverage on wind and wind-wave properties. *J. Oceanogr.*, **57**, 603–616.

Zhao, D., Y. Toba, K.-I. Sugioka, and S. Komori, 2006: New sea spray generation function for spume droplets. *J. Geophys. Res.*, **111**, C02007, doi: 02010.01029/02005JC002960.